



Cite this: *New J. Chem.*, 2019, 43, 16367

Organometal-catalyzed synthesis of high molecular weight poly-(L-lactic acid) with a covalently attached imidazolium salt: performance-enhanced reduced graphene oxide–PLLA biomaterials†

Yuri Clemente Andrade Sokolovicz,^{ib ab} Clarissa Martins Leal Schrekker,^{ib a} Frédéric Hild,^b Leonardo de Oliveira Bodo,^a Júlia Lacerda Couto,^a Joice Sandra Klitzke,^a Thuany Maraschin,^{ib c} Nara Regina de Souza Basso,^{ib c} João Henrique Zimnoch dos Santos,^{ib a} Samuel Dagorne^{ib *b} and Henri Stephan Schrekker^{ib *a}

Herein, we report on the synthesis of imidazolium salt end-functionalized PLLA (**PLLA-IS**) and its application in the preparation of reduced graphene oxide–PLLA composites. When applying the imidazolium salt 1-(2-hydroxyethyl)-3-methylimidazolium tetrafluoroborate as the initiator, the organometallic $Zn(C_6F_5)_2$ toluene complex polymerized L-lactide into high molecular weight **PLLA-IS** (M_n up to 56k). The presence of this imidazolium functionality enhanced the PLLA–reduced graphene oxide interaction, which promoted a homogenous dispersion of this filler when applying a solvent casting procedure. Significant improvements in the mechanical properties were achieved, reaching 148% and 105% for the loss and storage moduli, respectively. Besides, the **PLLA-IS/rGO-1%** composite inhibited the growth of fungal biofilms, including *C. tropicalis* (43%) and *C. albicans* (34%). Altogether, these materials exhibit properties for novel applications, including as biomaterials.

Received 31st July 2019,
Accepted 12th September 2019

DOI: 10.1039/c9nj03978c

rsc.li/njc

1. Introduction

Polyolefin-based thermoplastics are the most widely used polymers in our society and are widespread materials in all aspects of our daily life.^{1,2} In general, these polymers are made from petroleum-derived olefins being produced by the thermal breakdown of heavy hydrocarbons in steam catalytic cracking. This process requires a high temperature between 750 and 850 °C for the massive burning of fossil fuels, which results in large CO₂ emissions into the atmosphere.^{3,4} Although this issue could be minimized by the

use of renewable olefins, the accumulation of these non-biodegradable polyolefins in the environment would remain a problem.

Poly-(lactic acid) (PLA) is a biodegradable thermoplastic polyester material derived from the renewable resource lactic acid and has found several applications in the biomedical area and as a packaging commodity. Due to depletion of fossil resources, such a material is also considered as an alternative to petrochemically-sourced polyolefins. In this context, the ring opening polymerization (ROP) of lactide by well-defined metal-based catalysts has gained considerable attention to access PLA materials with controlled and possibly improved properties.⁵ Interestingly, in the ROP process an alcohol initiator may be covalently bonded to the PLA end-chain, which enables the addition of different functional end-groups by tuning the nature of the alcohol source.⁶

Low dimensional materials have been the driving force for various inventions and innovations, and are applied as nanofillers in polymer nanocomposites.⁷ Nanofillers like carbon nanotubes,⁸ graphene^{9–11} and nanosilica^{12,13} can improve the final properties of these nanocomposites, overcoming shortages of the polymer itself. Graphene is composed of one-atom-thick

^a Institute of Chemistry, Universidade Federal do Rio Grande do Sul, Porto Alegre, RS, Brazil. E-mail: henri.schrekker@ufrgs.br

^b Institute of Chemistry, Université de Strasbourg, CNRS, Strasbourg, France. E-mail: dagorne@unistra.fr

^c School of Technology, Pontifícia Universidade Católica do Rio Grande do Sul, Porto Alegre, RS, Brazil

† Electronic supplementary information (ESI) available: Reaction kinetics (Table 1, entry 13); MALDI-TOF mass spectrum of **PLLA-IS** (Table 1, entry 3) and proposed chemical structures; ¹H, ¹³C, ¹¹B and ¹⁹F NMR of **PLLA-IS** (Table 1, entry 15); ¹³C NMR of IS; photographs of rGO dispersion (**PLLA-IS/rGO-1%** and **PLLA/rGO-1%**); storage and loss moduli, and stiffness traces (**PLLA-IS** and **PLLA-IS/rGO-1%**); water contact angle micrographs (**PLLA-IS** and **PLLA-IS/rGO-1%**). See DOI: 10.1039/c9nj03978c

planar sheets of sp^2 -bonded carbon atoms and features outstanding mechanical, thermal¹⁴ and electrical¹⁵ properties. In particular, it is considered as one of the strongest materials ever tested with a breaking strength about two hundred times that of steel.¹⁴ Thus, while still in its infancy, the use of graphene as a nanocomponent in polymer composites holds great promise in terms of potential access to novel and improved materials.

Imidazolium salts (IS) are recognized as being suitable compatibilizing electrolyte agents due to the presence of surfactant-like cations and anions in their composition.¹⁶ These tunable salts have unique properties depending on the nature of the cation and anion, leading to a large array of applications with such entities,^{17,18} most notably in the nanocomposite^{19,20} and bioengineering²¹ fields. In our recent work, IS dispersed in a PLLA matrix increased the storage and loss moduli, thermal resistance, as well as the microbial antibiofilm inhibition of the final material.²² IS also exhibit potentially strong binding affinities with sp^2 -carbon-based nanostructures, and PLLA with a covalently attached IS (**PLLA-IS**) enhanced the dispersion of carbon nanotubes (CNT) in this polymeric matrix.²³

Few studies report on the synthesis and application of PLLA with graphene.²⁴ Recently, reduced graphene oxide (**rGO**) was applied as the initiator in the *L*-lactide ROP, resulting in the formation of PLLA nanocomposites with PLLA covalently bonded to **rGO**.²⁵ Other studies addressed the synthesis of PLLA/graphene nanocomposites through the solution mixing method.^{26–28}

Herein, we report for the first time the ROP of renewable *L*-lactide (**L-LA**) with an organometallic complex using an IS containing an alcohol group as the initiator to functionalize the PLLA chain with an IS-end group (**PLLA-IS**). The $Zn(C_6F_5)_2$ toluene complex catalyzed the ROP affording higher molecular weight **PLLA-IS**, which improved the interfacial interaction with reduced graphene oxide (**rGO**) (Fig. 1). Novel solvent-cast **PLLA-IS/rGO** bionanocomposites with performance-enhanced mechanical and thermal properties, and fungal antibiofilm activities were obtained, suggesting their potential application as biomaterials.

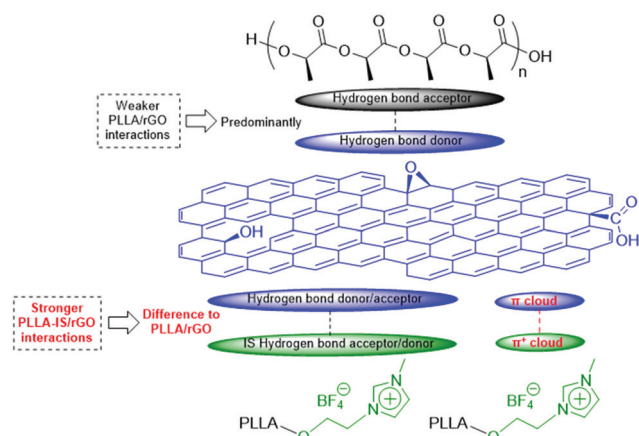


Fig. 1 The predominant interactions between **PLLA** and **rGO**, and the proposed differential interactions between **PLLA-IS** and **rGO** for the nanocomposites prepared in this study.

2. Experimental procedures

2.1 General considerations

All reactions and manipulations were performed under a N_2 atmosphere in a MBraun Unilab glovebox. Molecular sieves (4 Å) were activated under high vacuum at a temperature of 150 °C for at least 3 days. Dichloromethane (DCM), pentane and toluene were purchased from Sigma-Aldrich, and were first dried using a MBraun SPS purification system and then stored over activated molecular sieves (4 Å) for at least 20 h. Tetrahydrofuran (THF) was purchased from Sigma-Aldrich, distilled over Na/benzophenone and stored over activated molecular sieves (4 Å) for at least 48 h. Chloroform- d_1 and benzene- d_6 (C_6D_6) were purchased from Sigma-Aldrich and stored over activated molecular sieves (4 Å) for at least 20 h. PLLA (PURAPOL L100IXS) was provided by Corbion Purac. *L*-Lactide (**L-LA**) was purchased from Sigma-Aldrich and purified by recrystallization from toluene, and then sublimed in an inert atmosphere of N_2 . The chemical compounds diethylzinc ($ZnEt_2$) and tris(pentafluorophenyl)borane were purchased from Sigma-Aldrich, immediately stored inside the glovebox, and used as received. The imidazolium salt 1-(2-hydroxyethyl)-3-methylimidazolium tetrafluoroborate (**IS-OH**) was purchased from ABCR, dried under high vacuum for 48 h at 60 °C and then dried over activated molecular sieves (4 Å) for 5 days. The organometallic $Zn(C_6F_5)_2$ toluene complex was synthesized according to the procedure previously described in the literature.²⁹ Sulfuric acid (97%, Química Moderna), nitric acid (65%, Química Moderna) and hydrochloric acid (37%, Merck) were used as received. All other chemicals not described above were purchased from Sigma-Aldrich and used as received. The 1H and ^{13}C NMR spectra were recorded at room temperature on Bruker AC instruments (300, 400 and 500 MHz). Chemical shifts (δ) are given in parts per million (ppm) and referenced to $SiMe_4$ or residual solvent signals. GPC analyses of the polymer samples were all performed using a system equipped with a Shimadzu RID10A refractometer detector using HPLC-grade THF as an eluent (with molecular weights and polydispersity indices (PDIs) calculated using polystyrene standards). The molecular weight numbers (M_n) were corrected with appropriate correcting factors (0.58 for PLA) for the M_n values. Mass spectrometric analyses were performed using a MALDI-TOF PerSeptive Biosystems Voyager-DE STR mass spectrometer and the samples were analyzed with the DCTB “magic matrix” and KTFA.

2.2 General procedure for the synthesis of PLLA-IS

In a glovebox, the desired amounts of **IS-OH** and **L-LA** were weighed into a vial and diluted in toluene. The solution was kept under magnetic stirring until the total solubilization of the monomer. A toluene solution of the desired amount of $Zn(C_6F_5)_2$ toluene catalyst was then transferred to the vial and the reaction mixture heated to the desired temperature. After the time of interest, the solvent was removed under high vacuum and the **PLLA-IS** conversion was estimated using 1H NMR. The polymer product was dissolved in DCM and re-precipitated by addition of methanol, dried under high

vacuum for 6 h at 80 °C and fully characterized by ^1H , ^9F , ^{11}B and ^{13}C NMR; GPC and MALDI-TOF spectrometry.

2.3 General procedure for the synthesis of reduced graphene oxide (rGO)

The graphite (Grafine 99200, grain size 75 μm , Nacional de Grafite Ltda) was oxidized by the Staudenmaier method.³⁰ In this process, an acidic mixture of 160 mL of H_2SO_4 (97%) and 90 mL of HNO_3 (65%) was prepared in a reactor with a mechanical glass rod. The reactor was placed in an ice bath for 1 h to cool the system. After this period, graphite (10 g) was added to the acid mixture under constant stirring. Subsequently, 110 g of KCl_3 were added, and the reaction was continued for 24 h. To quench the reaction, 580 mL of an aqueous solution of HCl (10% by volume) were added to remove excess salts by centrifugation (5000 rpm, 15 min), and the supernatant was discarded. To obtain graphene oxide (GO), the precipitate was suspended in distilled water and placed in an ultrasound bath (40 kHz) for 4 h, and then the suspension was transferred to an osmotic membrane, which was dipped in a beaker with water. The water of the beaker was changed and the pH checked every 1 hour until the pH was 6. The GO suspension was dried in an oven at 150 °C. The resulting GO film was placed in a quartz ampoule and placed in a heating furnace. The thermal reduction of GO was carried out at a temperature of 1000 °C for 10 s to obtain rGO.

2.4 General procedure for the synthesis of PLLA-IS/rGO

0.5 g of PLLA-IS was weighed in a screw-capped vial, and 15 mL of CHCl_3 were added. This mixture was stirred for 10 min, and 5 mg of rGO (1 wt%) were added to the PLLA-IS solution. The final mixture was homogenized for 15 min under ultrasonication at 40 kHz and 60 °C for 1 h under stirring at room temperature. Finally, the mixture was poured into a mold and solvent cast to obtain a film of PLLA-IS/rGO-1%.

2.5 Thermogravimetric analysis (TGA)

TGA was performed using a Q50 TA Instruments equipment. The films were heated from 30 °C to 600 °C, at a heating rate of 20 °C min^{-1} . Analyses were conducted under a N_2 atmosphere with a gas flow rate of 60 mL min^{-1} . An average sample weight of 10 mg was analyzed in a platinum pan, and an empty pan was used as the reference.

2.6 Dynamic mechanical analysis (DMA)

DMA was performed using a Q800 TA Instruments equipment. Rectangular samples with a length of 11.6327 mm and a width of 6.9750 mm were tested in multifrequency strain mode by applying a tension of 125%. The moduli were tested in the range of 30–90 °C with a heating rate of 3 °C min^{-1} and at a constant and static force of 0.01 N. The storage modulus (E'), the loss factor δ (E''/E') and the loss modulus (E'') were recorded.

2.7 Water contact angle analysis

The water contact angles were determined using a Drop Shape Analyzer DSA100 (KRÜSS). An automated syringe deposited

deionized water (3 μL) on the samples. The contact angle was determined from the tangent line appropriately positioned on the contour of the drop in relation to the flat surface. The contact angles were measured using the software (Advance – Drop Shape) of the equipment.

2.8 Scanning electron microscopy (SEM) analysis

The morphological analysis of the films was performed using a JEOL JSM 6060 scanning electron microscope operating at 5 kV. The samples were placed on supports (stubs) with PELCO carbon conductive tape, and covered with a layer of carbon to increase the electrical conductivity.

2.9 Minor antibiofilm concentration assay

The capacity of the PLLA-IS films to inhibit the growth of biofilms was determined by the minor antibiofilm assay, following the protocols CLSI M27-A3 (<http://shop.clsi.org/microbiology-documents/M27.html>) and MM38-A2 (<http://shop.clsi.org/microbiology-documents/M38.html>) with modifications. Pure and young yeast colonies of the biofilm forming *Candida tropicalis* ATCC 13803 and *Candida albicans* ATCC 44858 species were grown in Petri dishes on Sabouraud agar with chloramphenicol at 36 °C for 24 h. This was followed by the preparation of a 10^6 colony forming unit (CFU) mL^{-1} yeast inoculum (100% transmittance for 0.9% saline and 90% transmittance for the 10^6 CFU mL^{-1} yeast inoculum) in sterile saline (0.9%). Aliquots of 20 μL were transferred into 96-well microplates and complemented with 180 μL of Roswell Park Memorial Institute (RPMI) culture medium. The PLLA-IS films (cut in circles of 5 mm in diameter) were sterilized by UV for 30 min, added, and incubated at 36 °C for 24 h. All samples were tested in quadruplicate. After removal of the PLLA-IS films from the wells, these were washed with 1 mL of sterile saline (0.9%) to remove nonadherent cells. Subsequently, the PLLA-IS films were placed in another 96-well microplate, followed by the addition of 160 μL of 3-(4,5-dimethylthiazol-2-yl)-2,5-diphenyltetrazolium bromide to stain the viable cells adhered to the materials. After 3 h, the 3-(4,5-dimethylthiazol-2-yl)-2,5-diphenyltetrazolium bromide solution was removed, and the PLLA-IS films were treated with 160 μL of isopropanol for 15 min. The absorption intensities at wavelengths of 570 and 690 nm were determined using a Biochrom EZ Read 400 microplate reader, using 100 μL samples of the each isopropanol solution. PLLA without IS was used as the positive control test (20 μL of yeast inoculum and 180 μL of RPMI). As a negative control, 200 μL of RPMI medium was applied.³¹ The following formula was used to determine the impediment percentage of biofilm formation on the PLLA-IS samples: $100 - \frac{[(\text{average assay absorbance})/(\text{average absorbance of the positive control})] \times 100}$.

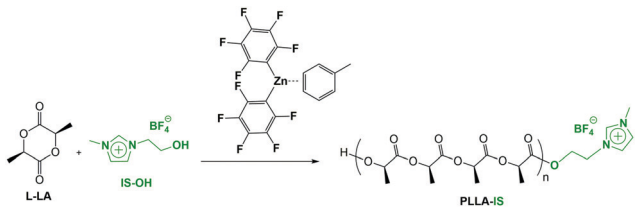
3. Results and discussion

The present study aimed at combining graphene dispersion capability and IS-functionalized PLLA antibiofilm properties to form a new reinforced biomaterial. IS-end-functionalized PLLA

(**PLLA-IS**) were shown to be accessible through ROP of lactide by organocatalytic routes, but only low molecular weight **PLLA-IS** – maximum of 10 000 g mol⁻¹.²³ Access to higher molecular weight PLLA in a controlled manner is best achieved using organometallic ROP catalysts. Nevertheless, access to **PLLA-IS** could not be achieved using the catalyst Sn(Oct)₂,³² the industrially implemented lactide ROP catalyst for PLLA synthesis.^{32,33} To date, access to **PLLA-IS** materials through organometallic routes has not been documented and would preferably involve cheap and earth-abundant metal sources. Accordingly, due to the lower toxicity of Zn (*vs.* Sn), the Zn-based lactide ROP is of current interest and, in that regard, we earlier reported that the Lewis acidic Zn(C₆F₅)₂ effectively polymerizes lactide in the presence of an alcohol initiator (such as BnOH) to produce BnO-end-functionalized PLLA.³⁴ Such an approach was further exploited to successfully prepare **PLLA-IS**, thus involving the ROP of *L*-lactide in the presence of an imidazolium alcohol moiety (**IS-OH**).

Species Zn(C₆F₅)₂(toluene) and 1-(2-hydroxyethyl)-3-methylimidazolium tetrafluoroborate (**IS-OH**) were used as the catalyst and initiator, respectively, for the ROP of *L*-lactide (**L-LA**). After an initial optimization process, the reaction temperature was set at 80 °C and toluene was chosen as the solvent, which led to the effective preparation of **PLLA-IS**, as deduced from the characterization data (NMR, MALDI-TOF, GPC). All ROP runs are compiled in Table 1 and were conducted with different catalyst/initiator/monomer ratios. The GPC traces are all monomodal and the relatively narrow polydispersities (*D* < 1.5) are in

Table 1 **L-LA** ROP catalyzed by Zn(C₆F₅)₂toluene/**IS-OH**^a



Entry	Zn/ IS-OH / L-LA	[L-LA]/ [IS-OH]	<i>t</i> ^b (min)	Conv. ^c (%)	<i>M</i> _{n,theor} ^d	<i>M</i> _n ^e	<i>D</i> ^f
1	1/3/150	50	45	90	6678	13 294	1.24
2	1/3/150	50	80	95	7049	15 200	1.12
3	1/3/200	66	60	95	9331	12 077	1.20
4	1/3/200	66	32	77	7563	8608	1.20
5	1/3/300	100	30	33	4827	6596	1.49
6	1/3/300	100	45	66	9654	13 208	1.37
7	1/3/300	100	50	91	13 310	10 450	1.51
8	1/3/300	100	80	97	14 188	19 372	1.44
9	1/3/300	100	100	97	14 188	21 140	1.51
10	1/5/300	40	32	74	6558	5773	1.17
11	1/3/600	200	45	30	8712	19 802	1.21
12	1/3/600	200	100	72	20 909	55 748	1.33
13	1/5/1000	200	6 h	97	28 169	48 181	1.50
14	1/10/1000	100	6 h	98	14 334	16 701	1.52
15	1/20/1000	50	6 h	98	7272	9044	1.35

^a Conditions: toluene, [**L-LA**]₀ = 1 M, 80 °C. ^b Reaction time in minutes. ^c **L-LA** conversion. ^d Theoretical *M*_n = [(*M*_L - *M*_{LA})₀ × *M*_w**L-LA**/(**IS-OH**)] + *M*_w**IL-OH** × conversion. ^e Measured by GPC in THF (30 °C), using a polystyrene standard and a correction factor of 0.58. ^f Polydispersity obtained by GPC in THF (30 °C).

line with a controlled ROP process. At lower initiator/catalyst ratios (Table 1, entries 1–9 and 11–12), the experimental *M*_n values were higher than the theoretical ones, which indicated a slower initiation *vs.* propagation in the present ROP process. The latter may be related to the steric hindrance of the **IS-OH** initiator. However, satisfyingly, higher initiator/catalyst ratios (Table 1, entries 14 and 15) resulted in PLA materials with good agreement between theoretical and experimental *M*_n values, suggesting that **IS-OH** acted as an effective polymer chain transfer agent as the ROP proceeded and that lactide ROP catalysis mediated by Zn(C₆F₅)₂/**IS-OH** may occur in an immortal manner. Indeed, the formation of chain-length-controlled **PLLA-IS** with *M*_n values matching the initial monomer/initiator ratio is characteristic of an immortal ROP process.³⁵ It is important that the use of Zn(C₆F₅)₂ as the catalyst provided for the first time access to high molecular weight **PLLA-IS**, with *M*_n up to 55 000 Da (Table 1, entry 12), which is of interest from an industrial point of view.

The controlled characteristic of the ROP process was further evidenced through kinetic studies: (i) a reaction rate with an observed first order in the monomer was observed with a 2–3 min induction period for ROP initiation (Fig. S1, ESI[†]); and (ii) a linear correlation between the **PLLA-IS**'s *M*_n and monomer conversion (Fig. S2, ESI[†]). These data confirmed a controlled immortal polymerization for the preparation of **PLLA-IS**.

The formation of imidazolium-end-functionalized PLLA was deduced from NMR data (Fig. S4–S8, ESI[†]) and MALDI-TOF spectrometric analysis (Fig. 2 and Fig. S3, ESI[†]). All these characterization data agree with the formation of PLLA chains covalently end-functionalized with the IS-O group (**PLLA-IS**). In particular, the MALDI-TOF mass spectrum presented in Fig. 2 is consistent with a Gaussian **PLLA-IS** product mass distribution, and the experimental mass values are in agreement with the calculated values (Fig. S3, ESI[†]). A second distinct distribution is visible and indicative of transesterification side reactions as the ROP proceeds. Such side reactions likely also rationalize the slightly broad polydispersity values of the produced **PLLA-IS** (Table 1).

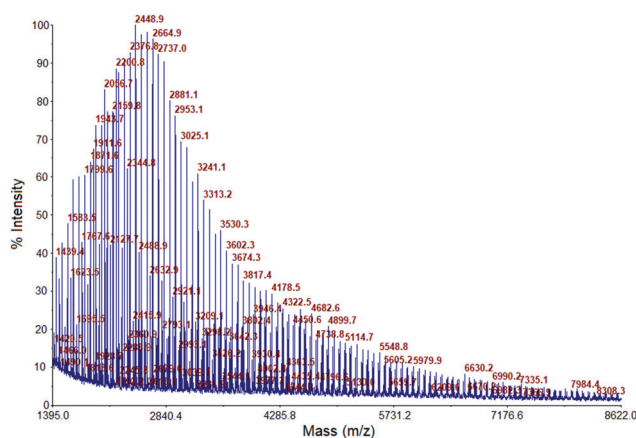


Fig. 2 Positive ion MALDI-TOF mass spectrum for **PLLA-IS** (DCTB magic matrix + KTFA). Conditions: **L-LA** (200 equiv.), [**L-LA**]₀ = 1 M, **IS-OH** (3 equiv.), Zn(C₆F₅)₂toluene (1 equiv.), 80 °C, toluene (Table 1, entry 3).

PLLA-IS (Table 1, entry 13) was applied in the solvent cast preparation of a novel **PLLA-IS/rGO** nanocomposite film containing 1 wt% of **rGO** (**PLLA-IS/rGO-1%**). This resulted in a good dispersion of the **rGO**, which was not the case when commercial PLLA with a similar molecular weight (to **PLLA-IS**) was used (Fig. S9, ESI†). In the case of PLLA, a phase separation was observed within a few minutes after pouring the mixture into the mold, indicating that the hydrogen bonding forces between PLLA (predominantly, hydrogen bond acceptor) and **rGO** (predominantly, hydrogen bond donor) are not enough to disperse **rGO** in the solution (Fig. 1). The good dispersion of **rGO** in **PLLA-IS** can be attributed to the differential intermolecular forces that result due to the presence of the IS unit. This involves low range $\pi^+-\pi$ interactions between the **PLLA-IS** imidazolium ring and the **rGO**, and hydrogen bonds between the IS unit (anion as the hydrogen bond acceptor and imidazolium ring hydrogen (especially at C2) as the hydrogen bond donor) and the **rGO** (both hydrogen bond donor and acceptor). The good dispersion remained when applying 10 wt% of **PLLA-IS**, in combination with 90 wt% of a commercial PLLA with a similar molecular weight, resulting in a homogeneous dispersion of the 1 wt% **rGO**.

Although hydrogen bonds are not formed between PLLA or **PLLA-IS** and carbon nanotubes, the $\pi^+-\pi$ interactions between the imidazolium ring of **PLLA-IS** and carbon nanotubes were strong enough to obtain nanocomposites with homogeneously dispersed carbon nanotubes.²³ As observed with **rGO**, PLLA did not disperse the nanocarbon tubes homogeneously.

SEM micrographs indicated a good interaction between the **PLLA-IS** polymer and **rGO**, indicating the formation of a controlled morphological structure of PLLA spheres which suggested their encapsulation into a **rGO** network (Fig. 3). The average size of these spheres was approximately 50 μm , and therefore they are considered microspheres. This morphological structure, the presence of IS, and the good graphene dispersion makes **PLLA-IS/rGO-1%** a potential material of interest for various applications.

The thermal properties of **PLLA-IS/rGO-1%** were compared with those of **PLLA-IS** (Table 2). With regard to the residual weight of 0.85 wt% at 550 °C, this was close to the theoretical value of 1.00 wt% for **PLLA-IS/rGO-1%**. The incorporation of **rGO** resulted in a significant gain of 15 °C for the $T_{50\%}$, which suggests that the **rGO** acted as a shield increasing the thermal resistance of encapsulated **PLLA-IS**. This improvement in thermal resistance is higher than that achieved when PLLA was covalently attached to **rGO** (1 wt%), which showed an increase of 10 °C.²⁵ This could be related to the location of the **rGO**: internal (covalently bonded PLLA) vs. external (non-covalently bonded PLLA). Compared to PLLA of similar molecular weight, **PLLA-IS** showed a lower initial thermal resistance ($T_{5\%}$), which improved at higher temperatures and resulted in higher $T_{10\%}$ and $T_{50\%}$ values.²² Although the dispersion of 2 wt% of IS in PLLA improved the thermal resistance,²² **PLLA-IS** showed a considerable increase of 24 °C in $T_{50\%}$.

The dynamic mechanical properties of **PLLA-IS** and **PLLA-IS/rGO-1%** were also investigated (Table 3). **PLLA-IS/rGO-1%**

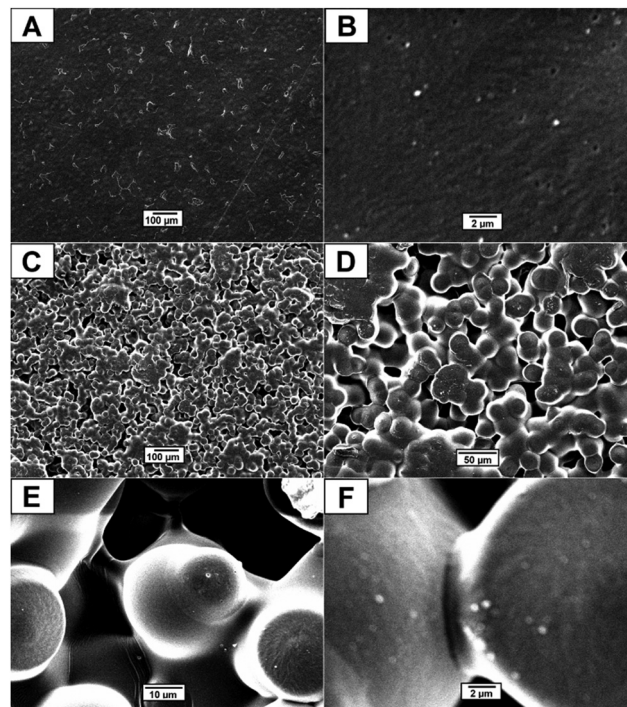


Fig. 3 SEM micrographs of (A) **PLLA-IS** (Table 1, entry 13) (scale bar = 100 μm); (B) **PLLA-IS** (scale bar = 2 μm); (C) **PLLA-IS/rGO-1%** (scale bar = 100 μm); (D) **PLLA-IS/rGO-1%** (scale bar = 50 μm); (E) **PLLA-IS/rGO-1%** (scale bar = 10 μm); and (F) **PLLA-IS/rGO-1%** (scale bar = 2 μm).

Table 2 Thermal properties of **PLLA-IS** films

Entry	Sample	$T_{5\%}^a$ [°C]	$T_{10\%}^b$ [°C]	$T_{50\%}^c$ [°C]	Residue ^d [%]
1	PLLA-IS ^e	151.2	291.3	367.4	0.00
2	PLLA-IS/rGO-1%	119.9	299.2	382.8	0.85

^a Temperature at 5 wt% weight loss as determined by TGA. ^b Temperature at 10 wt% weight loss as determined by TGA. ^c Temperature at 50 wt% weight loss as determined by TGA. ^d Residual weight at 550 °C as determined by TGA. ^e Table 1, entry 13.

showed an increase of 105% in the storage modulus when compared to **PLLA-IS** at 30 °C. Besides that, **PLLA-IS/rGO-1%** exhibited a significant increase of 148% in the loss modulus in comparison to **PLLA-IS** at 30 °C. The performance-enhanced mechanical properties of **PLLA-IS/rGO-1%** around the physiological temperature are of particular interest since such a biomaterial is commonly used as prosthesis in the human body. At higher temperature (55 °C), both films behave similarly for the storage and loss moduli. Compared to **PLLA-IS**, the stiffness of **PLLA-IS/rGO-1%** was 38% higher at 30 °C and 48% lower at 55 °C, and the T_g decreased by 5 °C. These results suggest that graphene promotes a greater PLLA chain-mobility and increases hardness, although the final material is less crumbly. Altogether, the presence of an IS group covalently bonded to PLLA led to a stronger, more rigid and less brittle material with 1 wt% of graphene.

The importance of this covalently attached IS-group is further supported by the dynamic mechanical properties of **PLLA/rGO** prepared *via* solution mixing, showing only minor

Table 3 Dynamic mechanical properties of PLLA-IS films

Entry	Sample	G'_{30^a} [Mpa]	G'_{55^b} [Mpa]	G''_{30^c} [Mpa]	G''_{55^d} [Mpa]	S_{30^e} [N M ⁻¹]	S_{55^f} [N m ⁻¹]	T_g^g [°C]
1	PLLA-IS ^h	386.9	241.4	25.6	34.1	42 097	26 259	64.8
2	PLLA-IS/rGO-1%	795.7	243.4	63.5	38.7	58 028	17 753	59.8

^a Storage modulus at 30 °C. ^b Storage modulus at 55 °C. ^c Loss modulus at 30 °C. ^d Loss modulus at 55 °C. ^e Stiffness at 30 °C. ^f Stiffness at 55 °C.

^g Glass transition temperature as determined by DMA. ^h Table 1, entry 13.

increases in storage and loss moduli, and stiffness.²⁶ This is most likely related to the weaker PLLA/rGO interaction (Fig. 1) and, as a consequence, the poorer rGO dispersion. Compared to PLLA with IS additives, PLLA-IS presented lower storage and loss moduli and higher stiffness and T_g , which can be ascribed to a lower chain mobility due to stronger IS-mediated intermolecular forces. This explains the formation of a weaker and more brittle material, which was partially recovered by the incorporation of 1 wt% rGO.

PLLA-IS had a water contact angle of 71.0°. This is close to that reported for PLLA (~69.5°), suggesting the same level of surface wettability.²² Although increasing contents of IS additives in PLLA resulted in reduced water contact angles,²² this was not observed with covalently IS end-functionalized PLLA. This indicated that the IS-group of PLLA-IS was preferentially located in the bulk away from the surface. A significant increase occurred with the incorporation of 1 wt% rGO as PLLA-IS/rGO-1% reached a water contact angle of 98.4°. This behavior can be explained by the presence of the hydrophobic graphene network around the polymer surface leading to a final material with a more hydrophobic character.

In this study, it was possible to verify that the antibiofilm activity of the imidazolium salt was maintained when covalently bound to the PLLA, which resulted in an inhibition percentage of 56% with *Candida tropicalis*. This percentage was somewhat lower when compared to PLLA with IS additives.²² This could be related to the preferential location of the IS-group in the respective materials: PLLA + IS (IS at the surface); PLLA-IS (IS in the bulk). Nevertheless, the *C. albicans* biofilm formation was not prevented by PLLA-IS. Interestingly, with the incorporation of graphene in the biomaterial, PLLA-IS/rGO-1% exhibited antibiofilm activity against both *C. tropicalis* (43%) and *C. albicans* (34%), which might be related to its higher hydrophobicity.

4. Conclusions

In conclusion, the synthesis of PLLA-IS with an organometallic complex – Zn(C₆F₅)₂toluene – as the catalyst and IS-OH as the initiator was performed using ROP for the first time. A higher molecular mass PLLA-IS product was prepared by this organometallic approach. The presence of an imidazolium end-group improved the dispersion of rGO, which resulted in the formation of a novel PLLA-IS/rGO biomaterial with better mechanical and thermal properties. In addition, this material was able to inhibit the formation of biofilms of *C. tropicalis* and *C. albicans*, exhibiting potential for application in medical devices and in the bioengineering field.

Conflicts of interest

There are no conflicts to declare.

Acknowledgements

We acknowledge Corbion Purac for donating PLLA, the Center of Microscopy and Microanalysis at UFRGS for the SEM facilities, and the Eindhoven University of Technology for the MALDI-TOF facilities. The Brazilian agencies Conselho Nacional de Desenvolvimento Científico e Tecnológico (CNPq; Science without Borders Special Visiting Scientist project 405784/2013-9), and Fundação de Amparo à Pesquisa do Estado do Rio Grande do Sul (FAPERGS, PqG project 17/2551-000-976-2) are acknowledged for financial support. This study was financed in part by the Coordenação de Aperfeiçoamento de Pessoal de Nível Superior – Brasil (CAPES) – Finance Code 001. J. H. Z. S., and H. S. S. are grateful to CNPq for the PQ fellowships. The University of Strasbourg and the CNRS are also acknowledged for financial support.

Notes and references

- 1 S. L. Aggarwal and O. J. Sweeting, *Chem. Rev.*, 1957, **57**, 665–742.
- 2 H. A. Maddah, *Am. J. Polym. Sci.*, 2016, **6**, 1–11.
- 3 Y. Yoshimura, N. Kijima, T. Hayakawa, K. Murata, K. Suzuki, F. Mizukami, K. Matano, T. Konishi, T. Oikawa, M. Saito, T. Shiojima, K. Shiozawa, K. Wakui, G. Sawada, K. Sato, S. Matsuo and N. Yamaoka, *Catal. Surv. Jpn.*, 2000, **4**, 157–167.
- 4 F. M. Alotaibi, S. González-Cortés, M. F. Alotibi, T. Xiao, H. Al-Megren, G. Yang and P. P. Edwards, *Catal. Today*, 2018, **317**, 86–98.
- 5 Recent representative reviews on metal-mediated ROP of lactide: (a) B. J. O'Keefe, M. A. Hillmyer and W. B. Tolman, *J. Chem. Soc., Dalton Trans.*, 2001, 2215–2224; (b) O. Dechy-Cabaret, B. Martin-Vaca and D. Bourissou, *Chem. Rev.*, 2004, **104**, 6147–6176; (c) R. H. Platel, L. M. Hodgson and C. K. Williams, *Polym. Rev.*, 2008, **48**, 11–63; (d) C. M. Thomas, *Chem. Soc. Rev.*, 2010, **39**, 165–173; (e) M. J. Stanford and A. P. Dove, *Chem. Soc. Rev.*, 2010, **39**, 486–494; (f) J.-C. Buffet and J. Okuda, *Polym. Chem.*, 2011, **2**, 2758–2763; (g) A. Sauer, A. Kapelski, C. Fliedel, S. Dagorne, M. Kol and J. Okuda, *Dalton Trans.*, 2013, **42**, 9007–9023; (h) S. Dagorne, M. Normand, E. Kirillov and J.-F. Carpentier, *Coord. Chem. Rev.*, 2013, **257**, 1869–1886; (i) S. Dagorne and C. Fliedel, *Top. Organomet. Chem.*, 2013, **41**, 125–172;

- (j) S. M. Guillaume, E. Kirillov, Y. Sarazin and J.-F. Carpentier, *Chem. – Eur. J.*, 2015, **21**, 7988–8003.
- 6 O. Dechy-Cabaret, B. Martin-Vaca and D. Bourissou, *Chem. Rev.*, 2004, **104**, 6147–6176.
- 7 For recent reviews on low dimensional materials see: (a) Y. Deng, Z. Liua, A. Wanga, D. Suna, Y. Chena, L. Yangb, J. Panga, H. Lic, H. Lid, H. Liua and W. Zhoua, *Nano Energy*, 2019, **62**, 338–347; (b) Z. Qua, L. Wua, B. Yuea, Y. Ana, Z. Liub, P. Zhaoc, J. Luoc, Y. Xied, Y. Liub, Q. Wanga, Z. Wanga, R. Daia and W. Yina, *Nano Energy*, 2019, **62**, 348–354; (c) K. Revathia, S. Palantavida and B. K. Vijayana, *Mater. Today: Proc.*, 2019, **9**, 587–593; (d) J. Pang, R. G. Mendes, A. Bachmatiuk, L. Zhao, H. Q. Ta, T. Gemming, H. Liu, Z. Liu and M. H. Rummeli, *Chem. Soc. Rev.*, 2019, **48**, 72–133; (e) M. Irfan, S. I. Bhat and S. Ahmad, *New J. Chem.*, 2019, **43**, 4706–4720; (f) M. Pusty, L. Sinha and P. M. Shirage, *New J. Chem.*, 2019, **43**, 284–294; (g) L. Suo, J. Zhao, X. Dong, X. Gao, X. Li, J. Xu, X. Lu and L. Zhao, *New J. Chem.*, 2019, **43**, 12126–12136; (h) Y. Xie, B. Liu, Y. Li, Z. Chen, Y. Cao and D. Jiaa, *New J. Chem.*, 2019, **43**, 12118–12125; (i) X. Hou, X. Liu, Z. Li, J. Zhang, G. Du, X. Ran and L. Yang, *New J. Chem.*, 2019, **43**, 13048–13057; (j) F. Shu, M. Wang, J. Pang and P. Yu, *Front. Chem. Sci. Eng.*, 2019, **13**(2), 393–399.
- 8 T. McDonnell and S. Korsmeyer, *Nature*, 1991, **354**, 56–58.
- 9 J. M. Raimond, M. Brune, Q. Computation, F. de Martini and C. Monroe, *Science*, 2004, **306**, 666–670.
- 10 H. Kim, A. A. Abdala and C. W. Macosko, *Macromolecules*, 2010, **43**, 6515–6530.
- 11 J. R. Potts, D. R. Dreyer, C. W. Bielawski and R. S. Ruoff, *Polymer*, 2011, **52**, 5–25.
- 12 B. Sun, G. Zhou and H. Zhang, *Prog. Solid State Chem.*, 2016, **44**, 1–19.
- 13 H. Zou, S. Wu and J. Shen, *Chem. Rev.*, 2008, **108**(9), 3893–3957.
- 14 A. A. Balandin, S. Ghosh, W. Bao, I. Calizo, D. Teweldebrhan, F. Miao and C. N. Lau, *Nano Lett.*, 2008, **8**, 902–907.
- 15 X. Du, I. Skachko, A. Barker and E. Y. Andrei, *Nat. Nanotechnol.*, 2008, **3**, 491–495.
- 16 Z. Lei, B. Chen, Y. M. Koo and D. R. Macfarlane, *Chem. Rev.*, 2017, **117**, 6633–6635.
- 17 R. L. Vekariya, *J. Mol. Liq.*, 2017, **227**, 44–60.
- 18 J. Lu, F. Yan and J. Texter, *Prog. Polym. Sci.*, 2009, **34**, 431–448.
- 19 S. Livi, J. Duchet-Rumeau and J. F. Gérard, *Macromol. Symp.*, 2014, **342**, 46–55.
- 20 B. G. Soares, *J. Mol. Liq.*, 2018, **262**, 8–18.
- 21 J. Claus, F. O. Sommer and U. Kragl, *Solid State Ionics*, 2018, **314**, 119–128.
- 22 C. M. L. Schrekker, Y. C. A. Sokolovicz, M. G. Raucchi, B. S. Selukar, J. S. Klitzke, W. Lopes, C. A. M. Leal, I. O. P. de Souza, G. B. Galland, J. H. Z. dos Santos, R. S. Mauler, M. Kol, S. Dagorne, L. Ambrosio, M. L. Teixeira, J. Morais, R. Landers, A. M. Fuentefria and H. S. Schrekker, *ACS Appl. Mater. Interfaces*, 2016, **8**, 21163–21176.
- 23 F. Meyer, J. Raquez, O. Coulembier, J. de Winter, P. Gerbaux and P. Dubois, *Chem. Commun.*, 2010, **46**, 5527–5529.
- 24 (a) P. Chen, Y. Wang, T. Wei, Z. Meng, X. Jia and K. Xi, *J. Mater. Chem. A*, 2013, **1**, 9028–9032; (b) M. Keramati, I. Ghasemi, M. Karrabi, H. Azizi and M. Sabzi, *Polym.-Plast. Technol. Eng.*, 2016, **55**(10), 1039–1047; (c) W. Li, Z. Xu, L. Chen, M. Shan, X. Tian, C. Yang, H. Lv and X. Qian, *Chem. Eng. J.*, 2014, **237**, 291–299; (d) Y. Sun and C. He, *ACS Macro Lett.*, 2012, **1**, 709–713.
- 25 J. Yang, S. Lin and Y. Lee, *J. Mater. Chem.*, 2012, **22**, 10805–10815.
- 26 D. Wu, Y. Cheng, S. Feng, Z. Yao and M. Zhang, *Ind. Eng. Chem. Res.*, 2013, **52**, 6731–6739.
- 27 H. S. Wang and Z. B. Qiu, *Thermochim. Acta*, 2011, **526**, 229–236.
- 28 H. S. Wang and Z. B. Qiu, *Thermochim. Acta*, 2012, **527**, 40–46.
- 29 D. A. Walker, T. J. Woodman, D. L. Hughes and M. Bochmann, *Organometallics*, 2001, **20**, 3772–3776.
- 30 M. J. McAllister, J. L. Li, D. H. Adamson, H. C. Schniepp, A. A. Abdala, J. Liu, M. Herrera-Alonso, D. L. Milius, R. Car, R. K. Prud'homme and I. A. Aksay, *Chem. Mater.*, 2007, **19**, 4396–4404.
- 31 E. A. Trafny, *Int. J. Occup. Med. Environ. Health*, 2013, **26**(1), 4–15.
- 32 T. Biedron, M. Brzezinski, T. Biela and P. Kubisa, *J. Polym. Sci., Part A: Polym. Chem.*, 2012, **50**, 4538–4547.
- 33 T. Biedron, Ł. Pietrzak and P. Kubisa, *J. Polym. Sci., Part A: Polym. Chem.*, 2011, **49**, 5239–5244.
- 34 G. Schnee, C. Fliedel, T. Avilés and S. Dagorne, *Eur. J. Inorg. Chem.*, 2013, 3699–3709.
- 35 N. Ajellal, J.-F. Carpentier, C. Guillaume, S. M. Guillaume, M. Helou, V. Poirier, Y. Sarazin and A. Trifonov, *Dalton Trans.*, 2010, **39**, 8363–8376.